Optical Engineering

OpticalEngineering.SPIEDigitalLibrary.org

Study on the roughness evolution of optical surfaces during ion beam sputtering

Xiao Liang
Xiang Wang
Yong-Qiang Gu
Jin-Jin Zheng
Huai-Jiang Yang
Yong-Xin Sui

SPIE.

Study on the roughness evolution of optical surfaces during ion beam sputtering

Xiao Liang,[a] Xiang Wang,[a,*] Yong-Qiang Gu,[b] Jin-Jin Zheng,[a] Huai-Jiang Yang,[b] and Yong-Xin Sui[b]
[a]University of Science and Technology of China, Department of Precision Machinery and Precision Instrumentation, 443 Huangshan Road, Hefei, Anhui 230026, China
[b]Chinese Academy of Sciences, Changchun Institute of Optics, Fine Mechanics and Physics, 3888 Dongnanhu Road, Changchun, Jilin 130033, China

Abstract. Ion beam machining technology has been extensively adopted to obtain an ultraprecision surface in ultraviolet lithography optics. However, there exist complex mechanisms leading the surface to evolve complicated topographies and increasing roughness. We build a kinetic model integrating with the typical sputter theory and a bond-counting Monte Carlo algorithm based on the compound materials to investigate the surface roughness evolution during ion beam sputtering. The influences of primary sputter, reflection, secondary sputter, geometrical shadowing, redeposition, and thermal diffusion were all taken into consideration to compose a dynamic evolution process. In calculation, using this model the surface first possesses a period of smoothing and then goes into a roughening stage, where the roughness follows the regular power law. Quantitative analyses of surface roughness derived from calculations are also examined and compared with experiments. © *2015 Society of Photo-Optical Instrumentation Engineers (SPIE)* [DOI: 10.1117/1.OE.54.10.104105]

Keywords: surface; roughness; topography; ion; sputtering; Monte Carlo.

Paper 150994 received Jul. 21, 2015; accepted for publication Sep. 11, 2015; published online Oct. 12, 2015.

1 Introduction

In the field of ultraviolet lithography optics, for the purpose of minimizing aberration and scattering on the surfaces of mirror substrates, a subnanometer-level surface precision over the entire range from low-spatial frequency figure to high-spatial frequency roughness has to be guaranteed in fabrication.[1,2] To achieve this aim, ion beam machining (IBM) technology based on physical sputter has increasingly been utilized to correct the figure error of optical surfaces.[3–5] However, the ion sputter process has a complex physics. During sputtering, the surface is far from equilibrium and a variety of atomistic mechanisms become effective which could either roughen or smooth the surface.[6,7] Since surface roughness of the substrate crucially influences the performance of the mirror, a three-dimensional (3-D) and atom-scale investigation of surface topography becomes essential. In this paper, we model the sputter-induced surface evolution based on the classical sputter theory and the bond-counting Monte Carlo algorithm on a binary surface represented by a quasiatomistic lattice. The dynamics of primary sputter, reflection, secondary sputter, geometrical shadowing, redeposition, and diffusion are integrated into this model.

2 Model

Here, a solid-on-solid cubic lattice shown in Fig. 1(a) is used to represent an amorphous surface configuration. The material is set as a binary compound A_aB_b and two-type atoms are distributed randomly at the ratio of $a:b$. Surface evolution is defined as a sputter-time dependent height function $H(x, y, t)$ $(1 \le x \le L,\ 1 \le y \le L)$, where the unit is the size of one cube (atom), i.e., L_d.

Below, the incidence and the reflection of the ion, the sputter, the redeposition, and the diffusion of surface atom are modeled in sequence and represented in the topography function $H(x, y, t)$. A previous version of our Monte Carlo algorithm of primary sputter has been introduced in Ref. 8, just as the $1^{\#}$ ion illustrated in Fig. 1(b). It bombards the surface site s at an incidence angle θ with respect to the macroscopic surface normal. It gives off its energy E at a penetration depth d in a Gaussian distribution, which has a parallel σ and a perpendicular width μ. The energy captured by the atom i (A or B) at site s' is ΔE_i:

$$\Delta E_i = \frac{E}{(2\pi)^{3/2}\sigma\mu^2} \cdot \exp\left\{-\frac{[d-z']^2}{2\sigma^2} - \frac{[x'^2+y'^2]}{2\mu^2}\right\}, \quad (1)$$

where (x', y', z') is the spatial coordinate of the site s' in the local Cartesian coordinate system $O'-X'Y'Z'$ where the axis Z' is along the incident trajectory. If the normal component $\Delta E_i \cdot \cos\beta_i$ to the local surface is larger than the surface binding energy U_i, the atom i is likely to be sputtered and the probability is proportional to $\Delta E_i \cdot \cos\beta_i$, where β_i is the exit angle of atom i with respect to the energy deposition orientation. We use the normalized Eq. (1) as the probability distribution function of sputtering a single atom off of the surface, that is, $P_i = \Delta E_i \cdot \cos\beta_i / \sum_{i=1}\Delta E_i \cdot \cos\beta_i$; hence, we can obtain the quantities and sites of these sputtered atoms by resampling the probabilities with random numbers for every ion. If some atom is judged to be sputtered, perform $H-1$ on the spot.

The ion could be reflected when the incident angle α with respect to the normal to the local surface is large enough.[9] If the reflected ion touches the surface again, it will cause secondary sputter (the same as the primary sputter in essence) as the $2^{\#}$ ion in Fig. 1(b). A study has shown an approximately exponential growth in the reflection probability with

*Address all correspondence to: Xiang Wang, E-mail: wxyf@ustc.edu.cn

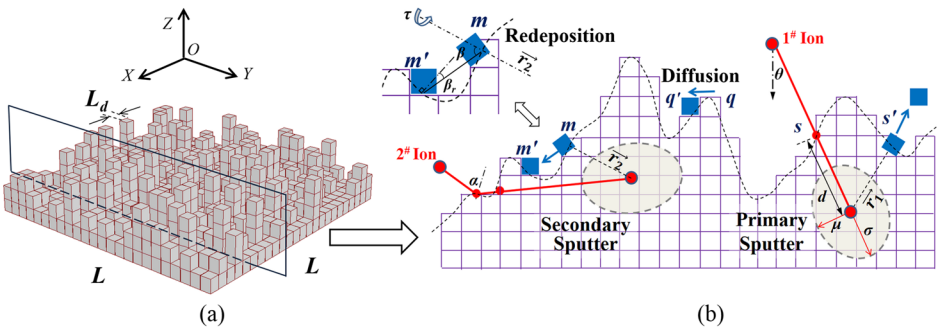

Fig. 1 Schematics of (a) the solid-on-solid model of material and (b) the incidence, energy distribution, primary sputter, redeposition, secondary sputter, and diffusion on the fitted surface.

increasing α (0 to 90 deg).[10] Thereafter, it is fitted as $\text{reflect}(\alpha) \approx 3.35e^{-6} \times \exp(0.14 \cdot \alpha) + 0.00672$. To reduce complexity, every ion is allowed to be reflected once at most and the energy loss is ignored. Here, we follow the rule of specular reflection.

A sputtered atom may redeposit back to the surface due to the surrounding topography. As shown in Fig. 1(b), the atom at site m, sputtered by the 2# ion, redeposits back to the surface at site m'. If there is no assistant gas involved, the adsorption ratio of the target for an approaching sputtered atom will be 100%.[11] Whether a sputtered atom will retouch the surface depends on its exit angle β, local surface profile, and the solid angle Ω covered by site m'. The distribution of β could be expressed as a cosine function $\cos\beta$.[12] According to the model setup, we have $\Omega = L_d^2 \cdot \cos\beta_r / d_m^2$, where d_m is the distance between m and m' and β_r is the redeposition angle, as shown in Fig. 1(b). The redeposition site m' is represented as a surface patch of $1\,L_d \times 1\,L_d$ and "2π" refers to the solid angle of hemisphere space. Thus, the redeposition probability of the sputtered atom redepositing at site m' can be written as

$$P_m = C_m \cdot \frac{\cos\beta}{\iint_{0<\beta<\pi,0<\tau<2\pi} \cos\beta \mathrm{d}\beta\,\mathrm{d}\tau} \cdot \left(\frac{\Omega}{2\pi}\right), \tag{2}$$

where τ is the rotation angle and C_m is a profile coefficient. If the sputtered atom from site m can fly directly to (shadowing) the other site m' without collision with other parts of the surface, $C_m = 1$, or else $C_m = 0$. Once the sputter site of some atoms is ensured, all the possible redeposition sites as well as the redeposition probabilities can be obtained according to a normalized Eq. (2). Similarly, resample the probabilities to determine the final redeposition site and then perform $H + 1$ on the spot. In this paper, we give the incident ions a certain flux and set the time scale of the model simulation through the sputter mechanism. Moreover, atomistic migration mimicking surface diffusion is also considered in the model as follows.

Atomistic diffusion is modeled as a thermally activated nearest neighbor jump process by overcoming some energy barriers between the start site and the target site.[13,14] Here, we employ a bond-counting Monte Carlo algorithm[15] to simulate it: we determine the number of nearest neighbors (bonds) of the atom at both the start site and the target site and then assign a generic diffusion rate modified by the change in the number of bonds, so we can utilize the rates of possible events to ensure the final jump event via sampling. For the atom j (A or B) moving from site q to its neighbor site q', the total energy barrier is $E_j = E_0 + (N_j - N_j{}')E_b$, where E_0 is the activation energy for a migration without breaking any bond and E_b is bond energy. Notice that the bond energies of an A—A, A—B, or B—B bond are set to the same value for the sake of complexity reduction. N_j and $N_j{}'$ refer to the number of bonds of each site and we have $N_j - N_j{}' = 0$ for $N_j{}' \geq N_j$, which means no bonds are broken. Therefore, the Arrhenius-form rate of the atom diffusing from q to the neighboring q' is $R_j = f_0 \cdot \exp\{-E_j/k_BT\}$, where k_B is the Boltzmann constant, h is the Planck constant, T is the temperature, and $f_0 = 2k_BT/h$. If we incorporate the factor $\exp\{-E_0/k_BT\}$ into the rescaled attempt frequency, $f_1 = (2k_BT/h) \cdot \exp\{-E_0/k_BT\}$ can be regarded as the attempt frequency of surface diffusion.[16] So, we have $R_j = f_1 \cdot \exp\{-(N_j - N_j{}')E_b/k_BT\}$. Then the probability of the atom diffusing from q to q' can be expressed as its rate share among its all possible jump events, that is, $P_j = R_j/\sum_{j=1} R_j$.[15] Thus, we can obtain the probability of every possible jump for each surface atom. At each diffusion step, one jump event is chosen to occur. Next we resample the probabilities to determine the final jump atom and final jump event and then perform $H - 1$ at the start site and perform $H + 1$ at the final site on the spot.

Therefore, the main simulation flow can be described as

1. Pick a position in $L \times L$ randomly and start an ion incidence.
2. Judge whether the ion is reflected. If reflected, go to step (3); or else go to step (4).
3. Judge whether secondary sputter occurs. If not, go to step (1); if yes, go to step (4).
4. Resample to determine and perform sputter events.
5. Judge whether redeposition occurs for each sputtered atom. If occurs, perform them.
6. Repeat steps (1) to (5) until the count reaches $0.000167L^2$ and then resample to determine and perform diffusion events.
7. Run statistics and go back to step (1).

3 Results and Discussions

Based on this model, a series of sputter simulations in conditions of different ion incidence angles on a random surface

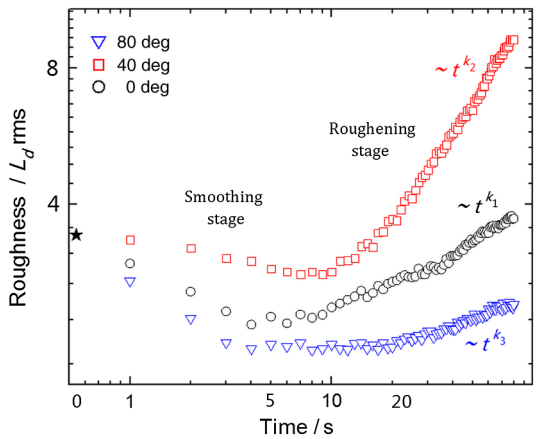

Fig. 2 Time-dependent surface roughness based on the whole $512\,L_d \times 512\,L_d$ surface, under 0-, 40-, and 80-deg incidence, in the double logarithmic coordinate. The pentagram indicates the initial roughness value—3.42 L_d rms.

sized of $512\,L_d \times 512\,L_d$ was conducted. To contact the experimental conditions, we must adopt reliable material properties and experimental parameters. In this paper, the substrate material was assumed as A_1B_2 (i.e., $a = 1$, $b = 2$) and the length unit was equivalent to 1 $L_d = 3.5$ Å = 0.35 nm, which conforms to the typical amorphous material—fused silica with an interatomic distance of 1.5 to 5.5 Å. Thus, the surface binding energies (U_a and U_b) were set to 4.6 and 2.6 eV, respectively, as fused silica. The energy distribution lengths, that is, d, σ, $\mu = 10, 5, 4\,L_d$ were from the literature.[8] As to the diffusion part, the temperature was taken to 400 K and the barriers also referenced the literatures:[16,17] E_0, $E_b = 0.75, 0.2$ eV. Typically, in IBF experiments, we have $\eta = 10^{15}$atoms $\cdot$ cm^{-2} on the surface, such as quartz glasses, and have a commonly used ion energy $E = 600$ eV. Since the typical experimental ion current density is of the order $F = 10^{15}$ ions $\cdot$ cm^{-2} s^{-1}, this implies an ion flux of $\Phi = F/\eta \sim 1$ ions atom^{-1} $\cdot$ s^{-1}, which is adopted in this paper to set the time scale of simulation. In addition, from the values given above, we can get a jump attempt frequency $f_1 \approx 6000$ s^{-1}, which means around 6000 diffusion steps/s occur. Thus, in order to facilitate the calculation, we initiate a diffusion step for every $\Phi L^2/f_1 = 0.000167\,L^2$ ion incidence steps.

The basic sputter part of this model can present a consistent energy dependency and angular dependency coinciding with the Sigmund sputter theory. Next, the combined effect is studied. For the initial random surface, the roughness is 3.42 L_d rms (~1.20 nm rms) and its peak-to-valley difference value is within 40 L_d. The surface roughness $Rq(t)$s derived from the whole $512\,L_d \times 512\,L_d$ surface under three incidence angles of 0, 40, and 80 deg, are presented in Fig. 2 (three angles represent three typical conditions of normal, oblique, and glancing incidence, respectively). The schematic plots of local topographies with the horizontal length of 128 L_d, when $t = 0$ (i.e., initial), 5, 10, and 20 s, are exhibited in Fig. 3.

On the condition of normal incidence ($\theta = 0$ deg), we can see from Fig. 2 that the surface is smoothed before about 5 s. During this period, the observed major changes are shrinking hills (e.g., $A_1 \rightarrow A_1'$) and widening valleys (e.g., $A_2 \rightarrow A_2'$) as shown in Figs. 3(a) and 3(b) ("→" means evolving from the former to the latter). However, the surface gradually enters a roughening stage after about 5 s and the roughness increases with time as a power law $Rq(t) \sim t_1^k$, where k_1, called the "roughness exponent," is 0.305. In this stage, when the biggish hills remain shrunken, new hills appear in surface depressions (e.g., A_3), thus the spatial frequency of surface topography becomes higher as shown in Figs. 3(b) and 3(c). As the ion dose continues to increase, new hills become spinier (e.g., $A_3 \rightarrow A_3'$) and the valleys are deepened (e.g., $A_4 \rightarrow A_4'$), as shown in Figs. 3(c) and 3(d). These simulation results suggest that in the early sputter stage, when ions are normally incident, surface regions sloped to the incident ion beam are eroded faster than a relatively planar region due to the shorter energy deposition depth, resulting in a successive lateral shrinkage of surface protrusions. The slope-dependent sputter effect dominates the early surface evolution and leads to a net smoothing. As shown by Carter,[18] this effect tends to erode existing surface protrusions with a high aspect ratio much faster than surface depressions. In our model, the centers of energy deposition are defined to always be below the surface with a certain depth, so the sputter rate could depend on the local surface curvature so that the regions at the top of surface hills (positive curvature) sputter more slowly than the regions in the valleys (negative curvature), according to Bradley and Harper's opinions.[19] This differentiated sputter could cause surface valleys to be deepened and increase surface roughness. Thus, as ions sequentially impinge, when those towering protrusions fade away, this local curvature-dependent sputter effect gradually dominates and turns the late surface evolution into a roughened status.

For comparison purposes, a series of experiments were performed. A Kaufman-type Ar^+ ion beam with an energy of 600 eV and an ion current density of $\sim 1 \times 10^{15}$atoms $\cdot$ cm^{-2} $\cdot$ s^{-1} was applied vertically onto the fused silica surface with an initial roughness of about 1.26 nm rms. We know there is consistency in the atomistic length unit (1 $L_d = 0.35$ nm), ion energy, ion flux, and initial roughness (1.20 nm rms ≈ 1.26 nm rms). Here, we utilize surface roughness to perform a comparative analysis between the simulation and experimental results. Figure 4 shows that the experimental result displays a similar trend to the simulation result in that surface roughness first falls and then rises with time. Furthermore, the experimental roughness also follows a power law $Rq(t) \sim t^{0.411}$ in the roughening stage with an exponent of 0.411, which is a little larger than the exponent 0.305 derived from simulation. Indeed, there is a certain difference between the experimental data and simulated values in spite of the consistent trend. The error sources could be the magnitude difference between the experiment area (in the range of millimeters) and the simulation area (in the range of micrometers), could be the difference in the initial surface topography between the experiment and simulation, and/or could be the fact that the energy deposition centers of partial ions could not always be under the surface in practice.

As to the condition of oblique incidence (40 deg), at first the surface is in a smoothing stage until about 8 s. In this period, Figs. 3(e)–3(g) show some smoothing phenomena such as biggish hills being shrunken (e.g., $B_1 \rightarrow B_1' \rightarrow B_1''$). Then the surface shifts into a roughening stage after about 10 s and the roughness increases as $Rq(t) \sim t_2^k$, where the exponent k_2 is 0.752. In the roughening period, the

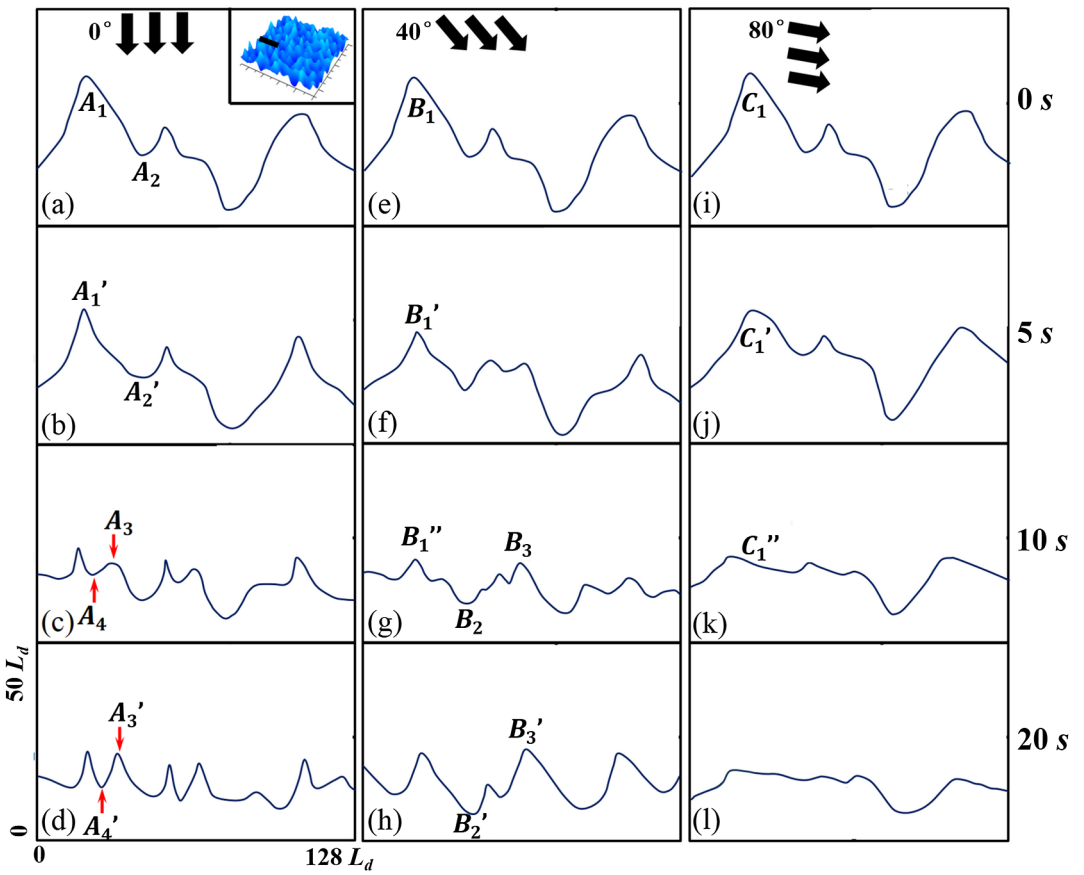

Fig. 3 Schematics of local topographies with the horizontal length of 128 L_d, when the time is (a, e, and i) 0, (b, f, and j) 5 s, (c, g, and k) 10 s, and (d, h, and l) 20 s, and the incidence angle is (a–d) 0 deg, (e–h) 40 deg, and (l, j, k, and l) 80 deg. The inset is the corresponding 512^2 surface. The black arrow indicates the projection direction and the black line-segment indicates the location of local topographies.

valleys are deepened (e.g., $B_2 \rightarrow B_2'$) and the hills grow again in amplitude (e.g., $B_3 \rightarrow B_3'$). Furthermore, the surface topography has a directional and periodic tendency as in Fig. 3(h), where the average spatial wavelength of these ripples is 18.1 to 19.5 nm. The emergence of this type of periodic surface pattern demonstrates that the surface sputtered by oblique incident ions reaches a balance between the roughening processes (local curvature dependent sputter) and the smoothing processes (local slope-dependent sputter, redeposition, surface diffusion, etc.). The formation mechanism of a microcosmic ripple caused by such a balance has been given a conforming description in the B-H model.[19] This featured ripple-like profile in our simulation that often appears in the surface morphologies of glass materials after ion beam irradiation.[20–22] A similar experiment based on amorphous SiO_2 by Toma et al.[23] shows an increasing roughness as a power law with a larger exponent of 1.02 (ours is 0.752) and shows a ripple with a wavelength of around 17.2 nm at about 20 s, which is a bit less than our 18.1 to 19.5 nm. The differences in value should be connected with the higher ion energy—800 eV in their experiments because the ripple wavelength is often found to decrease with energy[6] and the surface roughness generally increases with energy.[24]

When ions are incident at a glancing angle of 80 deg, the surface remains smoothed for a long time, as shown in Fig. 2. Although there exists an increase in roughness after 10 s following the power law $Rq(t) \sim t_3^k$, the roughness exponent is very small ($k_3 = 0.103$). Before 10 s, we can intuitively see from Figs. 4(i)–4(k) that the biggish protrusions are preferentially removed (e.g., $C_1 \rightarrow C_1' \rightarrow C_1''$) and the planar regions expand on the surface. The surface evolution is apparently dominated by a geometrical shadowing effect and preferential removal of the glancing incidence to be smoothed. Subsequently, facing a relatively flat surface, the reflection probability of the glancing ion increases, so

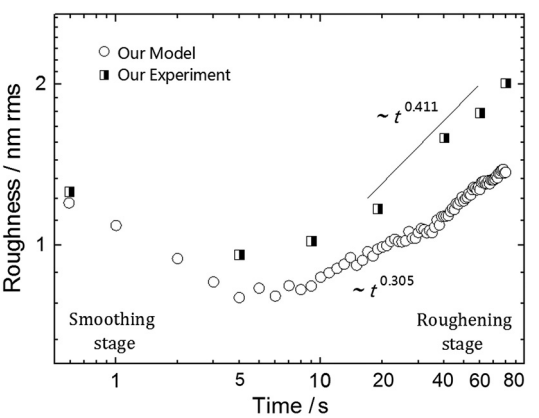

Fig. 4 Comparisons of surface roughness between experiments (measured by the white light interferometer) and simulations under normal incidence.

that surface protrusions are more likely to be secondarily sputtered by the reflected ions and could be further planarized. In addition, the enhanced ion backscattering induced by surface reflection reduces the removal rate (or sputter yield), just as with the small profile variation shown between Figs. 3(k) and 3(l). The featured geometrical shadowing and preferential removal at a glancing incidence are also consistent with many experimental observations of large-angle ion beam processing.[25–27]

4 Conclusion

In Summary, a kinetic model with 3-D simulations was used to investigate the surface roughness and topography evolution for an ion beam sputtering process. The kinetics of ion sputter, secondary sputter, redeposition, and thermal diffusion were integrated in this model. The results of simulations show that, dominated by different atomistic surface processes, the surface always exhibits a two-stage evolution with time—from smoothing to roughening, and in the late roughening stage surface, roughness always follows the regular power law. These results were consistent with our and others' experimental observations. This model provides an efficient approach to understand the mechanism for the roughness evolution of the ion-irradiated surface and can give a certain assistance and guidance in predicting and handling the roughness problem in IBM for ultra-accuracy and ultra-smooth optical substrates.

Acknowledgments

This study is financially supported by NSFC-CAS Joint Fund (Grant No. U1332130), 111 Projects (Grant No. B07033), 973 Project (Grant No. 2014CB931804), and the State Key Laboratory of Applied Optics (China).

References

1. B. Wu and A. Kumar, "Extreme ultraviolet lithography: a review," *J. Vac. Sci. Technol. B* **25**, 1743 (2007).
2. M. J. Lercel et al., "EUV lithography with the alpha demo tools: status and challenges," *Proc. SPIE* **6517**, 651706 (2007).
3. A. Schindler et al., "Ion beam and plasma jet etching for optical component fabrication," *Proc. SPIE* **4440**, 217–227 (2001).
4. W. Liao et al., "Corrective capability analysis and machining error control in ion beam figuring of high-precision optical mirrors," *Opt. Eng.* **51**(3), 033402 (2012).
5. T. Arnold et al., "Ultra-precision surface finishing by ion beam and plasma jet techniques—status and outlook," *Nucl. Instrum. Methods A* **616**, 147 (2010).
6. W. L. Chan and E. Chason, "Making waves: kinetic processes controlling surface evolution during low energy ion sputtering," *J. Appl. Phys.* **101**, 121301 (2007).
7. P. Mishra and D. Ghose, "Effect of initial target surface roughness on the evolution of ripple topography induced by oxygen sputtering of Al films," *J. Appl. Phys.* **105**, 014304 (2009).
8. X. Liang et al., "An investigation on the removal characteristics of compound materials during ion beam sputtering using the kinetic Monte Carlo method," *Nucl. Instrum. Methods B* **323**, 1–6 (2014).
9. S. Lindsey and G. Hobler, "The significance of redeposition and backscattering in nanostructure formation by focused ion beams," *Nucl. Instrum. Methods B* **282**, 12–16 (2012).
10. C. Ebm and G. Hobler, "Assessment of approximations for efficient topography simulation of ion beam processes: 10 keV Ar on Si," *Nucl. Instrum. Methods B* **267**, 2987–2990 (2009).
11. J. Sun et al., "An investigation of redeposition effect for deterministic fabrication of nanodots by focused ion beam," *Precis. Eng.* **36**, 31–36 (2012).
12. H. B. Kim et al., "Simulation of ion beam induced micro/nano fabrication," *J. Micromech. Microeng.* **17**, 1178–1183 (2007).
13. P. Šmilauer, M. Wilby, and D. Vvedensky, "Reentrant layer-by-layer growth: a numerical study," *Phys. Rev. B* **47**, 4119–4122 (1993).
14. R. Lam and D. G. Vlachos, "Multiscale model for epitaxial growth of films: growth mode transition," *Phys. Rev. B* **64**, 035401 (2001).
15. J. B. Adams, Z. Wang, and Y. Li, "Modeling Cu thin film growth," *Thin Solid Films* **365**, 201–210 (2000).
16. E. O. Yewande, A. Hartmann, and R. Kree, "Propagation of ripples in Monte Carlo models of sputter-induced surface morphology," *Phys. Rev. B* **71**, 195405 (2005).
17. E. Chason and B. K. Kellerman, "Monte Carlo simulations of ion-enhanced island coarsening," *Nucl. Instrum. Methods B* **127**, 225 (1997).
18. G. Carter, "The physics and applications of ion beam erosion," *J. Phys. D: Appl. Phys.* **34**, R1 (2001).
19. R. M. Bradley and J. M. E. Harper, "Theory of ripple topography induced by ion bombardment," *J. Vac. Sci. Technol. A* **6**, 2390 (1988).
20. A. Keller, S. Facsko, and W. Möller, "Evolution of ion-induced ripple patterns on SiO2 surfaces," *Nucl. Instrum. Methods B* **267**, 656 (2009).
21. A. Keller, S. Facsko, and W. Möller, "The morphology of amorphous SiO2 surfaces during low energy ion sputtering," *J. Phys.* **21**, 495305 (2009).
22. J. Völlner et al., "Topography evolution mechanism on fused silica during low-energy ion beam sputtering," *J. Appl. Phys.* **109**, 043501 (2011).
23. A. Toma et al., "Ion beam erosion of amorphous materials: evolution of surface morphology," *Nucl. Instrum. Methods B* **230**, 551–554 (2005).
24. S. A. Pahlovy et al., "Roughening and smoothing behavior of single crystal Si by low energy Ar+ ion bombardment," *Nucl. Instrum. Methods B* **272**, 206–209 (2012).
25. M. Wißing, M. Batzill, and K. J. Snowdon, "Preparation by glancing incidence ion irradiation of surfaces with ångstrom-scale RMS roughness," *Nanotechnology* **8**(1), 40 (1997).
26. K. Kimura et al., "Preparation of smooth Si(0 0 1) surfaces by glancing angle sputtering," *Nucl. Instrum. Methods B* **148**, 149–153 (1999).
27. T. Hino et al., "Smoothing of polycrystalline copper with rough surface by oblique argon-ion irradiation," *J. Vac. Sci. Technol. B* **24**, 1918 (2006).

Xiao Liang received his bachelor's degree from the University of Science and Technology of China (USTC), Hefei, China, in 2011. He is currently pursuing a PhD at USTC. His research interests include optical precision fabrication and ion beam machining.

Xiang Wang received his PhD from USTC in 2003. He has been an associate professor and the leader of the Laboratory of Advanced Manufacturing Technology at USTC. His research interests include optical manufacturing, micro/nanofabrication, and rapid prototyping.

Yong-Qiang Gu received his PhD in 2013 from Changchun Institute of Optics, Fine Mehcanics and Physics (CIOMP). He is now working at CIOMP. His research interest is ultraprecision optical machining.

Jin-Jin Zheng received his PhD in 1998 from the University of Birmingham. He is currently a professor and the director of the Laboratory of Computer Aided Design and Manufacturing, USTC. His research interests include computer-aided manufacturing, graphic and image processing technology, and precision fabrication.

Huai-Jiang Yang received his PhD in 1996 from Beijing Institute of Technology (BIT). He is currently a senior research scientist and the academic leader at CIOMP. His research interests include optical manufacturing and detection, spectral imaging, and nanoprecision drive control and application.

Yong-Xin Sui received his PhD in 2002 from CIOMP. He is currently a senior research scientist at CIOMP. His research interests include optical detection, optical information fusion, and optical information security.